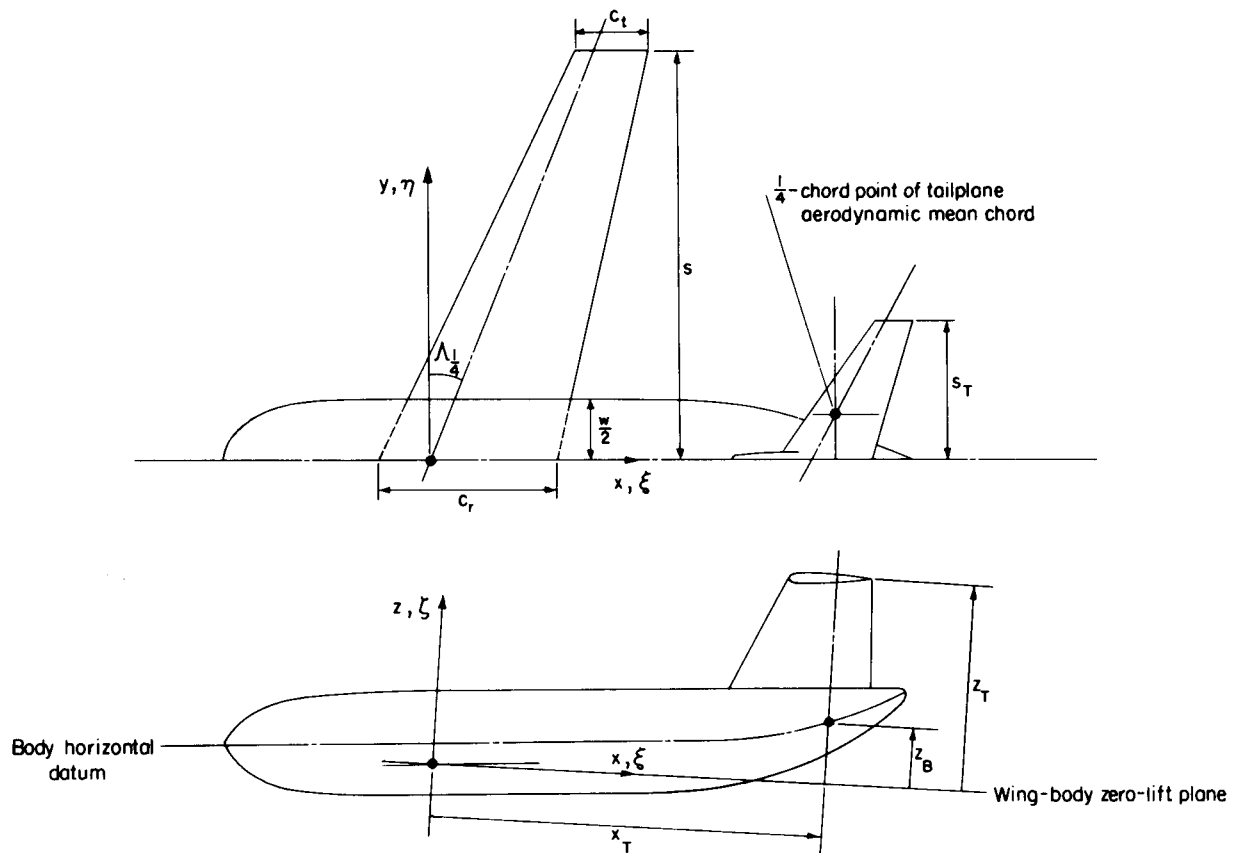# AVERAGE DOWNWASH AT THE TAILPLANE AT LOW ANGLES OF ATTACK AND SUBSONIC SPEEDS

1. NOTATION AND UNITS (see Sketch 1.1)

		SI	British
A	aspect ratio of wing planform, $4s^2/S$		
B	factor for body effect on average downwash gradient, see Equation (3.3)		
a_1	wing lift-curve slope	radian^{-1}	radian^{-1}
c_r	wing root (centre-line) chord	m	ft
c_t	wing tip chord	m	ft
$\bar{\bar{c}}$	aerodynamic mean chord of wing	m	ft
F	downwash averaging factor, see Equation (4.1)		
H_p	downwash parameter on centre line ($\eta = 0$, $\zeta = 0$,) of plane vortex sheet, see Equation (4.2)	radian	radian
H_{pe}	downwash parameter for wing with elliptic loading	radian	radian
$H_{p\infty}$	value of H_p as $\xi \to \infty$	radian	radian
ΔH_p	correction to H_p	radian	radian
K_M	factor for Mach number effect on average downwash gradient, see Section 7		
M	free-stream Mach number		
$R_{\bar{\bar{c}}}$	Reynolds number based on $\bar{\bar{c}}$		
S	wing planform area	m^2	ft^2
s	wing semi-span	m	ft
s_T	tailplane semi-span	m	ft
w	maximum width of body	m	ft
x, y, z	orthogonal co-ordinates with origin at quarter-chord point of wing centre-line chord; x-axis located on intersection of plane of symmetry and wing-body zero-lift plane		

x_T	distance of tailplane behind quarter-chord point of wing centre-line chord	m	ft
z_B	height of body centre line above x-axis	m	ft
z_T	height of tailplane above x-axis	m	ft
α	angle of attack measured from datum, body horizontal datum, for example	degree	degree
α_0	angle of attack for zero wing-body lift	degree	degree
ε	downwash angle	degree	degree
$\bar{\varepsilon}$	average downwash angle across tailplane mounted on wing-body combination, see Section 3	degree	degree
$\bar{\varepsilon}_0$	value of $\bar{\varepsilon}$ at zero wing-body lift	degree	degree
$\Lambda_{\frac{1}{4}}$	sweepback angle of wing quarter-chord line	degree	degree
$\Lambda_{\frac{1}{2}}$	sweepback angle of wing half-chord line	degree	degree
λ	ratio of wing tip chord to centre-line (root) chord, c_t/c_r		
$\xi, \eta, \zeta,$	$x/s, y/s, z/s$		
$\xi_T, \eta_T, \zeta_T,$	$x_T/s, s_T/s, z_T/s$		
ζ_B	z_B/s		

Superscript

*	denotes wing-tail combination

Subscripts

M	denotes Mach number
0	denotes $\zeta_T = 0$

Note: To cater for other than straight-tapered planforms the equivalent wing planform concept described in Item No. 76015 (Derivation 26) should be used.

Sketch 1.1

2.   INTRODUCTION

This Item gives data for the average downwash at the tailplane for subsonic speeds and low angles of attack where the lift, pitching moment and downwash characteristics are linear, *i.e.* where the flow is wholly attached. Under these conditions it is a good approximation to assume that up to the location of the tailplane the vortex sheet shed from the wing will be substantially flat, and this assumption is inherent to that part of the method used in this Item which is theoretically based. Under these conditions, and up to the location of the tailplane, it will be assumed that the vortex sheet shed from the wing trailing edge lies in the zero-lift plane for the wing-body combination, and this is taken as the datum from which to measure tailplane height.

Section 3 gives the basis of the method while Sections 4 and 5 detail the methods whereby the downwash expressions in Section 3 may be evaluation for low-speed flows. A brief discussion of the effects of nacelles is given in Section 6. The effects of compressibility are assessed in Section 7. The accuracy and applicability of the method are outlined in Section 8 and a detailed worked example is given in Section 10. (Item No. 97021 deals with the effect of trailing-edge flap deployment on the average downwash at the tailplane at low speeds.)

3. BASIS OF THE METHOD

At low angles of attack, where the lift and pitching moment characteristics are linear, the average downwash at the tailplane (see Sketch 3.1) is given by

$$\bar{\varepsilon} = \varepsilon_0 + \left(\frac{d\bar{\varepsilon}}{d\alpha}\right)(\alpha - \alpha_0) \tag{3.1}$$

where $\bar{\varepsilon}_0$ is the value of $\bar{\varepsilon}$ at zero wing-body lift (*i.e.* at $\alpha = \alpha_0$) and $d\bar{\varepsilon}/d\alpha$ is the average downwash gradient appropriate to the tailplane mounted on a wing-body combination.
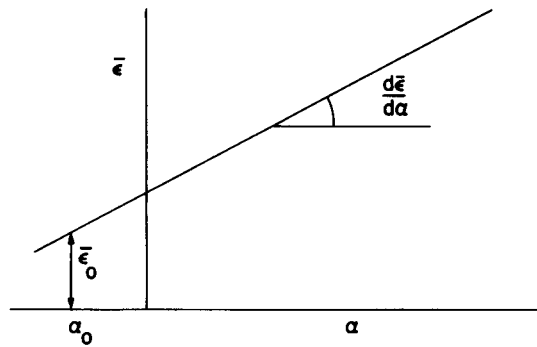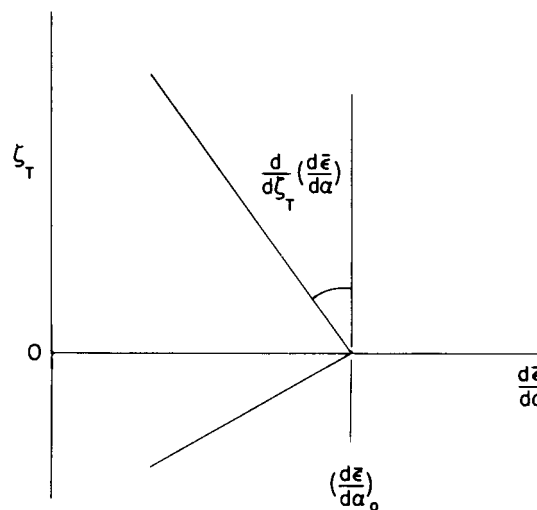

Sketch 3.1

For the purposes of a downwash calculation the tailplane is assumed to be located on the lateral axis passing through the quarter-chord point of the aerodynamic mean chord of the tailplane at a distance ζ_T downstream of the quarter-chord point of the wing centre-line chord.

If a linear variation in average downwash gradient with tail height, ζ_T, is assumed (see Sketch 3.2)

$$\frac{d\bar{\varepsilon}}{d\alpha} = \left(\frac{d\bar{\varepsilon}}{d\alpha}\right)_0 - \left|\,\zeta_T\,\right|\left|\,\frac{d}{d\zeta_T}\left(\frac{d\bar{\varepsilon}}{d\alpha}\right)\,\right|. \tag{3.2}$$

Sketch 3.2

4

Now the term $(\mathrm{d}\bar{\varepsilon}/\mathrm{d}\alpha)_0$ in Equation (3.2) can be expressed in the form

$$\left(\frac{\mathrm{d}\bar{\varepsilon}}{\mathrm{d}\alpha}\right)_0 = B \times \left(\frac{\mathrm{d}\bar{\varepsilon}}{\mathrm{d}\alpha}\right)_0^* \tag{3.3}$$

in which $B = \dfrac{(\mathrm{d}\bar{\varepsilon}/\mathrm{d}\alpha)_0}{(\mathrm{d}\bar{\varepsilon}/\mathrm{d}\alpha)_0^*}$ and the superscript * denotes the value for a wing-tail combination.

Combination of Equations (3.2) and (3.3) gives

$$\frac{\mathrm{d}\bar{\varepsilon}}{\mathrm{d}\alpha} = B \times \left(\frac{\mathrm{d}\bar{\varepsilon}}{\mathrm{d}\alpha}\right)_0^* - \left|\ \zeta_T\ \right|\left|\ \frac{\mathrm{d}}{\mathrm{d}\zeta_T}\left(\frac{\mathrm{d}\bar{\varepsilon}}{\mathrm{d}\alpha}\right)\right|\ . \tag{3.4}$$

4. EVALUATION OF EQUATION (3.4) FOR DOWNWASH GRADIENT AT LOW SPEEDS

4.1 Downwash Gradient at Zero Tailplane Height (first term in Equation (3.4))

The average downwash gradient at the tailplane of a wing-tail combination when the tailplane is immersed in the wing vortex sheet $(\zeta_T = 0)$ may be estimated using the following equation developed in Derivation 29. The equation, which assumes a flat vortex sheet, was derived using the method of Derivation 19, in which the spanwise loadings were given by lifting-surface theory for the series of wing planforms in Derivation 22, together with an empirical correction.

$$\left(\frac{\mathrm{d}\bar{\varepsilon}}{\mathrm{d}\alpha}\right)_0^* = \frac{2}{\pi}\frac{a_1}{A}(H_p + \Delta H_p)F \tag{4.1}$$

where $\qquad F = \left(\dfrac{\mathrm{d}\bar{\varepsilon}/\mathrm{d}\alpha}{\mathrm{d}\varepsilon/\mathrm{d}\alpha}\right)_0^*$

and $\qquad H_p = H_{pe} - (1 - H_{p\infty})\,. \tag{4.2}$

Values of a_1/A are obtained from Item No. 70011 (Derivation 23) for *incompressible flow*, $M = 0$; compressibility effects are dealt with in Section 7. Figures 1a to 1d present data for $H_{p\infty}$, the downwash parameter at an infinite distance downstream $(\xi_T \to \infty)$ on the centre line $(\eta_T = 0, \zeta_T = 0)$ of the vortex sheet shed from the wing. Figure 2 presents the variation of the downwash parameter H_{pe} with downstream distance from the quarter-chord point of the wing centre-line chord (ξ_T) and the quarter-chord sweep $(\Lambda_{1/4})$ for a flat vortex sheet behind an elliptically-loaded wing. Figure 3 provides an empirically-derived correction, ΔH_p, to give good agreement with experimental downwash gradient data for wing-tail combinations[†], (Derivations 1, 2, 3 and 7).

Figures 4 to 7 present the factor, F, to apply to the centre-line downwash gradient to estimate the average downwash gradient across the tailplane span. The factors were calculated for tailplanes located one wing semi-span downstream (*i.e.* $\xi_T = 1$) but they are not very sensitive to variation in ξ_T over the usual range for tailplane location $(0.5 \le \xi_T \le 2)$. For wings with elliptic loading the factor is close to unity.

The factor B, accounting for the effect of the body on the average downwash gradient at the tailplane, is given by Figure 8 which was obtained from a correlation of experimental data for wing-body-tail combinations (Derivations 2, 5, 8 to 18, 21,25, 27 and 30) having values of $w/2s$ ranging from 0.1 to 0.2.

[†] The tailplane in these cases was usually attached to the wing with a very slender boom assumed to provide negligible interference with the wing downwash field.

4.2 Effect of Tailplane Height on Downwash Gradient (second term in Equation (3.4))

The rate of change of average downwash gradient at the tailplane with tailplane height, $\left|d(d\bar{\varepsilon}/d\alpha)/d\zeta_T\right|$, assumed independent of tailplane height, is obtained from the empirically-derived curve in Figure 9 for wing-body-tail combinations (Derivations 2, 6, 8 to 15, 18, 21, 25, 27 and 30) having values of $w/2s$ in the range 0.1 to 0.2. The experimental data were found to correlate rather better when the effects of planform were taken out via a_1/A (obtained from Derivation 23) and when the effects of tailplane span were taken out via the downwash averaging factor, $F^{\dagger}$. The curve given is appropriate to high tailplanes $(\zeta_T > 0)$. For low tailplanes $(\zeta_T < 0)$ the indications are that a factor of about 1.3 should be applied to the values of $\left|d(d\bar{\varepsilon}/d\alpha)/d\zeta_T\right|$ obtained from Figure 9.

5. LOW SPEED DOWNWASH AT ZERO LIFT

The zero-lift value of the average downwash at the tailplane, $\bar{\varepsilon}_0$, may be influenced by a number of parameters. They include tailplane location, afterbody geometry, wing twist, wing-body setting angle and junction design, in addition to Reynolds number. Investigation of a number of experimental data indicated that the most significant single parameter is the height of the tailplane above the body centre-line, $\zeta_T - \zeta_B$, see Sketch 1.1. The curve given in Figure 10 is the mean line drawn through the data (Derivations 2, 4, 5, 8 to 18, 21, 25, 27, 28 and 30) and represents the trend with variation in tailplane height quite well although the scatter of the experimental data about the mean is large (about ± 1 degree). Further attempts to reduce the scatter by identifying other parameters felt to be significant proved unsuccessful, largely owing to the ad hoc nature of the test data. It is not, therefore, currently possible to predict $\bar{\varepsilon}_0$ to any great accuracy.

6. EFFECT OF NACELLES

The addition of engine nacelles can have a very significant effect on the downwash at the tailplane. Very few data (Derivation 30) are available on which to base an assessment of nacelle effect.

For rear-fuselage mounted nacelles, from the results for four models, there is a consistent increase in average downwash gradient at the tailplane ranging from 0.02 to 0.08, with a mean value of 0.06. The effect on average downwash at zero wing-body lift for these nacelles ranges from 0.1 to –0.8 degrees with a mean value of about –0.2 degrees. These values should be used only as a guide to the magnitude of the likely effects of adding rear-fuselage mounted nacelles.

For under-wing mounted nacelles the data, from only two models, are inconclusive in that there are opposing signs between the models for the effects on both downwash gradient and downwash at zero wing-body lift.

7. EFFECT OF COMPRESSIBILITY

Figure 11 provides an estimate of the effect of Mach number on $d\bar{\varepsilon}/d\alpha$ up to that at which the aerodynamic characteristics start to diverge rapidly. The factor K_M $(=(d\bar{\varepsilon}/d\alpha)_M/(d\bar{\varepsilon}/d\alpha)_{M=0})$ in Figure 11 has been derived empirically from relatively few test data in Derivations 4, 17 and 27.

The effect of compressibility on $\bar{\varepsilon}_0$ can be assumed to be insignificant up to the divergence Mach number defined in the previous paragraph.

[†] Note that the use of this factor, corresponding to $\zeta_T = 0$ implicitly assumes that it is applicable to tail heights other than zero, which is not a bad approximation for the range of tail heights in practice $(-0.1 < \zeta_T < 0.5)$.

8. ACCURACY AND APPLICABILITY

8.1 Accuracy

The method of Section 4 predicts 93 per cent of the experimental values of $d\bar{\varepsilon}/d\alpha$ at low speeds for wing-body tail combinations to within ±20 per cent, while 70 per cent are predicted to within ±10 per cent. The effects of compressibility are predicted by Figure 11 to within about ±6 per cent up to the Mach number at which the aerodynamic characteristics start to diverge rapidly.

The experimental data for $\bar{\varepsilon}_0$ for wing-body-tail combinations are predicted by Figure 10 to within ± 1 degree independent of Mach number.

8.2 Applicability

The method of this Item is essentially a first-order one allowing for the major effects of wing planform, body, wing-body interference and tailplane height. In this respect the method has been developed assuming a planar vortex sheet and as such ought not to apply to twisted wings, for example. However, a number of the test models used in the accuracy assessment of Section 8.1 had wings with varying amounts of twist and the values of $d\bar{\varepsilon}/d\alpha$ and $\bar{\varepsilon}_0$ for these models were generally predicted with errors well within the maximum scatter band and were fairly evenly distributed. This being so the method may be assumed to apply to configurations with moderate amounts of twist.

The data given in this Item are applicable to wing-body-tail combinations at low angles of attack where the lift, pitching moment and downwash characteristics are linear, *i.e.* where the flow is wholly attached. The Item is also applicable up to the Mach number for the aircraft at which the aerodynamic characteristics start to diverge rapidly with increase in Mach number.

The Item applies only to wing-body-tail configurations although some assessment of the effect of rear-fuselage mounted nacelles is given in Section 6.

Forty five wind-tunnel models were used in the studies for this Item covering the parameter ranges shown in Table 8.1.

TABLE 8.1 Parameter Ranges Covered by the Item

A	λ	$\Lambda_{\frac{1}{4}}$	$w/2s$	ξ_T	η_T	ζ_T	$R_{\bar{\bar{c}}} \times 10^6$
2	0	0	0.1	0.5	0.2	–0.2	0.5
to	to	to	to	to	to	to	to
12	1	52	0.2	3	0.8	0.6	15

9. DERIVATION

The Derivation lists selected sources that have assisted in the preparation of this Item.

1. PIERCY, N.A.V. — On the flow in the rear of an aerofoil at small angles of incidence. ARC R & M 578, 1918.

2. BLACKBURN AIRCRAFT LTD — Investigation of the effect of full span, high-lift flaps on the flow in the region of the tailplane, and upon stability and trim. Part I: without slipstream. Blackburn Aircraft Rep. WT 88/43 (ARC 7115), 1943.

3. TRIENES, H. — Systematic measurements of downwash behind sweptback wings. AITHB Rep. 45/8. (Abstracted in RAE tech. Note Aero 1819, 1946 by H.M. Lyon.)

4. LINDEMANN, H. — Systematische Abwindmessungen bei hohen Unterschall-geschwindigkeiten. Volkenrode R & T 603, 1947. (Translation available as "Systematic downwash measurements at high subsonic speeds", RAE Lib. Trans. 198, 1947.)

5. TROUNCER, J. / MOSS, G.F. — Low speed wind-tunnel tests on two 45 deg sweptback wings of aspect ratios 4.5 and 3.0 (Models A and B). ARC R & M 2710, 1947.

6. PURSER, P.E. / SPEARMAN, M.L. / BATES, W.R. — Preliminary investigation at low speed of downwash characteristics of small-scale swept-back wings. NACA tech. Note 1378, 1947.

7. LOCK, R.C. / ROSS, J.G. / MEIKLEM, P. — Wind tunnel test on a 90° apex delta wing of variable aspect ratio (sweepback 36.8°). Part II – Measurements of downwash and effect of high lift devices. ARC CP83, 1948.

8. SALMI, R.J. — Horizontal-tail effectiveness and downwash surveys for two 47.7° sweptback wing-fuselage combinations with aspect ratios of 5.1 and 6.0 at a Reynolds of 6.0×10^6. NACA RM L50K06 (TIL 2600), 1950.

9. GRINER, R.F. / FOSTER, G.V. — Low speed longitudinal and wake air-flow characteristics at a Reynolds number of 6.0×10^6 of a 52° sweptback wing equipped with various spans of leading-edge and trailing-edge flaps, a fuselage, and a horizontal tail at various vertical positions. NACA RM L50K29 (TIL 2633), 1950.

10. SALMI, R.J. / JACQUES, W.A. — Effect of vertical location of a horizontal tail on the static longitudinal stability characteristics of a 45° sweptback-wing-fuselage combination of aspect ratio 8 at a Reynolds number of 4×10^6. NACA RM L51J08 (TIL 2993), 1951.

11. JACQUET, B.M. — Effects of horizontal-tail position, area, and aspect ratio on low-speed static longitudinal stability and control characteristics of a 60° triangular-wing model having various triangular-all-movable horizontal tails. NACA RM L51106 (TIL 2971), 195l.

12. FOSTER, G.V. / GRINER, R.F. — Low speed longitudinal and wake air-flow characteristics at a Reynolds number of 5.5×10^6 of a circular-arc 52° sweptback wing with a fuselage and a horizontal tail at various vertical positions. NACA RM L51C30 (TIL 2790), 1951.

13. GRAHAM, D.
    KOENIG, D.G.

    Tests in the Ames 40-by 80- foot wind tunnel of an airplane configuration with an aspect ratio 4 triangular wing and an all-movable horizontal tail – longitudinal characteristics. NACA RM A51H10a (TIL 2896), 1951.

14. GRAHAM, D.
    KOENIG, D.G.

    Tests in the Ames 40-by 80- foot wind tunnel of an airplane configuration with an aspect ratio 2 triangular wing and an all-movable horizontal tail – longitudinal characteristics. NACA RM A51B21 (TIL 2704), 1951.

15. FRANKS, R.W.

    Tests in the Ames 40- by 80- foot wind tunnel of two airplane models having aspect ratio 2 trapezoidal wings of taper ratios 0.33 and 0.20. NACA RM A52L16 (TIL 3611), 1952.

16. KOENIG, D.G.

    Tests in the Ames 40-by 80- foot wind tunnel of an airplane configuration with an aspect ratio 3 triangular wing and an all-movable horizontal tail – longitudinal and lateral characteristics. NACA RM A52L15 (TIL 3687), 1952.

17. TINLING, B.E.
    LOPEZ, A.E.

    The subsonic static aerodynamic characteristics of an airplane model having a triangular wing of aspect ratio 3. I – effects of horizontal-tail location and size on the longitudinal characteristics. NACA tech. Note 4041, 1953.

18. BANDETTINI, A.
    SELAN, R.

    The effects of horizontal-tail height and a partial-span leading-edge extension on the static longitudinal stability of a wing-fuselage-tail combination having a sweptback wing. NACA RM A53J07 (TIL 4114), 1953.

19. DeYOUNG, J.
    BARLING, W.H.

    Prediction of downwash behind swept-wing airplanes at subsonic speed. NACA tech. Note 3346, 1954.

20. DECKER, J.L.

    Prediction of downwash at various angles of attack for arbitrary tail locations. *Aero. Engng. Rev.* Vol. 15, No. 8, pp.22 to 27 and 61, August 1956.

21. LOVELL, D.A.

    A low-speed wind-tunnel investigation of the tailplane effectiveness of a model representing the Airbus type of aircraft. RAE tech. Rep. 69077, 1969.

22. GARNER, H.C.
    INCH, S.M.

    Subsonic theoretical lift-curve slope, aerodynamic centre and spanwise loading for arbitrary aspect ratio, taper ratio and sweepback. ARC CP1137, 1970.

23. ESDU

    Lift-curve slope and aerodynamic centre position of wings in inviscid subsonic flow. Item No. 70011. Engineering Sciences Data Unit, London, July 1970.

24. FINK, M.P.
    SHIVERS, J.P.
    SMITH, C.C.

    A wind-tunnel investigation of static longitudinal and lateral characteristics of a full-scale mockup of a light twin-engine airplane. NASA tech. Note D-6238, 1971.

25. KIRBY, D.A.
    HEPWORTH, A.G.

    Low-speed wind-tunnel tests of the longitudinal stability characteristics of some swept-wing quiet Airbus configurations. RAE tech. Rep. 76029, 1976.

26.   ESDU   Aerodynamic centre of wing-fuselage combinations. Item No. 76015. Engineering Sciences Data Unit, London, September 1976.

27.   AEROSPATIALE   Unpublished wind-tunnel data from Aérospatiale, Toulouse, France.

28.   ARA   Unpublished wind-tunnel data from Aircraft Research Association, Bedford.

29.   CHAPPELL, P.D.   Average downwash at the tailplane. Memor. No. 39. Engineering Sciences Data Unit, London, September 1980,

30.   BAe   Unpublished wind-tunnel data from British Aerospace, Aircraft Group, Weybridge-Bristol, Hatfield-Chester and Manchester Divisions.

10.   EXAMPLE

Find the average downwash gradient at the tailplane at low angles of attack and a Mach number of 0.8 for the wing-body-tail combination depicted in Sketch 10.1. Find also the average downwash angle at the tailplane corresponding to the zero wing-body lift condition.
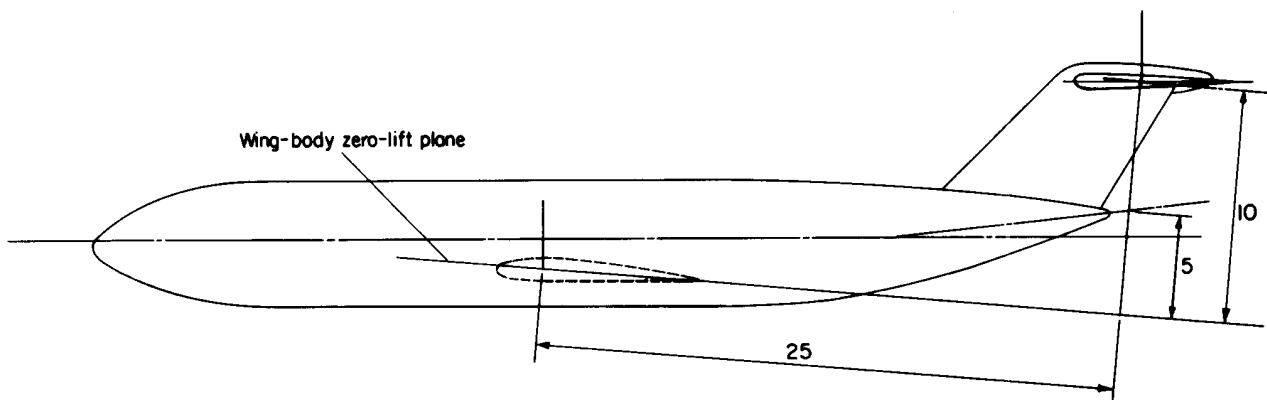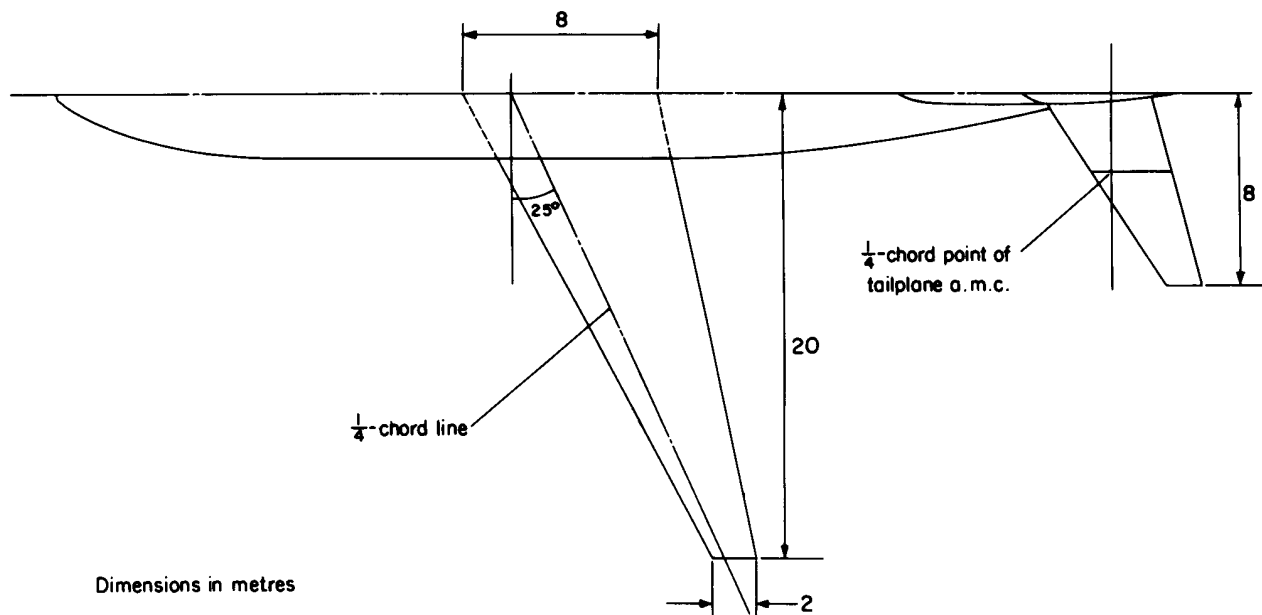
Sketch 10.1

From Sketch 10.1 the various geometrical parameters required can be calculated as follows:

$$A = 4\ s^2/S = 4 \times 20^2 \Big/ \frac{(8+2)}{2} \times 20 \times 2 = 8 \ .$$

$$\lambda = c_t/c_r = 2/8 = 0.25.$$

$$A\tan\Lambda_{\frac{1}{2}} = A\tan\Lambda_{\frac{1}{4}} - \frac{1-\lambda}{1+\lambda} = 8 \times \tan 25° - \left(\frac{1-0.25}{1+0.25}\right) = 3.13 \ .$$

$$\tan\Lambda_{\frac{1}{4}} = \tan 25° = 0.466.$$

$$\xi_T = x_T/s = 25/20 = 1.25.$$

$$\eta_T = s_T/s = 8/20 \ \ = 0.4.$$

$$\zeta_T = z_T/s = 10/20 = 0.5.$$

$$\zeta_B = z_B/s = 5/20 \ \ = 0.25.$$

From Item No. 70011 for $A = 8$, $A\tan\Lambda_{\frac{1}{2}} = 3.13$ and $\lambda = 0.25$ the value of a_1/A for $M = 0$ (*i.e.* $\beta A = 8$) is 0.565 rad^{-1}.

From Figure 1b for $A = 8$ and $A\tan\Lambda_{\frac{1}{2}} = 3.13$, $H_{p\infty} = 1.02$ radians. From Figure 2 for $\tan\Lambda_{\frac{1}{4}} = 0.466$ and $1/\xi_T = 1/1.25 = 0.8$, $H_{pe} = 1.10$ radians.

Therefore, from Equation (4.2), $H_p = H_{pe} - (1 - H_{p\infty}) = 1.10 - (1 - 1.02) = 1.12$ radians.

From Figure 3 for $A = 8$ and $H_{p\infty} = 1.02$ radians, $\Delta H_p = -0.12$ radians.

From Figures 4b to 7b for $A = 8$ and $\eta_T = 0.4$:

$A\tan\Lambda_{\frac{1}{2}}$	F
0	0.915
2	0.975
4	1.012
6	1.056

From a plot of these data an interpolation for $A\tan\Lambda_{\frac{1}{2}} = 3.13$ gives $F = 0.995$.

Therefore, from Equation (4.1)

$$\left(\frac{d\bar{\varepsilon}}{d\alpha}\right)_0^* = \frac{2}{\pi}\frac{a_1}{A}(H_p + \Delta H_p)F = \frac{2}{\pi} \times 0.565 \times (1.12 - 0.12) \times 0.995 = 0.358 \ .$$

From Figure 8 for $A = 8$, $B = 1.37$.

Therefore $(d\bar{\varepsilon}/d\alpha)_0 = B \times (d\bar{\varepsilon}/d\alpha)_0^* = 1.37 \times 0.358 = 0.490$.

Now $\dfrac{(d\bar{\varepsilon}/d\alpha)_0}{(a_1/A)F} = \dfrac{0.490}{0.565 \times 0.995} = 0.872$ radians .

Therefore from Figure 9 with this abscissal value,

$$\left|\frac{\mathrm{d}}{\mathrm{d}\zeta_T}\left(\frac{\mathrm{d}\bar{\varepsilon}}{\mathrm{d}\alpha}\right)\right|\bigg/\left(\frac{a_1}{A}F\right) = 0.940 \text{ radians}.$$

Thus $\left|\dfrac{\mathrm{d}}{\mathrm{d}\zeta_T}\left(\dfrac{\mathrm{d}\bar{\varepsilon}}{\mathrm{d}\alpha}\right)\right| = 0.940 \times 0.565 \times 0.995 = 0.528$.

From Equation (3.2) the average low-speed downwash gradient at the tailplane for $\zeta_T = 0.5$ is

$$\begin{aligned}
\frac{\mathrm{d}\bar{\varepsilon}}{\mathrm{d}\alpha} &= \left(\frac{\mathrm{d}\bar{\varepsilon}}{\mathrm{d}\alpha}\right)_0 - 0.5 \times \left|\frac{\mathrm{d}}{\mathrm{d}\zeta_T}\left(\frac{\mathrm{d}\bar{\varepsilon}}{\mathrm{d}\alpha}\right)\right| \\
&= 0.490 - 0.5 \times 0.528 \\
&= 0.226 = (\mathrm{d}\bar{\varepsilon}/\mathrm{d}\alpha)_{M=0}.
\end{aligned}$$

From Figure 11 the factor for compressibility at $M = 0.8$ is $K_M = 1.19$.

Therefore the average downwash gradient at the tailplane for $M = 0.8$ is

$$\left(\frac{\mathrm{d}\bar{\varepsilon}}{\mathrm{d}\alpha}\right)_{M=0.8} = K_M \times \left(\frac{\mathrm{d}\bar{\varepsilon}}{\mathrm{d}\alpha}\right)_{M=0} = 1.19 \times 0.226 = 0.269.$$

Finally, from Figure 10, for $\zeta_T - \zeta_B = 0.5 - 0.25 = 0.25$, the average downwash at the tailplane corresponding to zero wing-body lift is $\bar{\varepsilon}_0 \approx 1.8$ degrees.
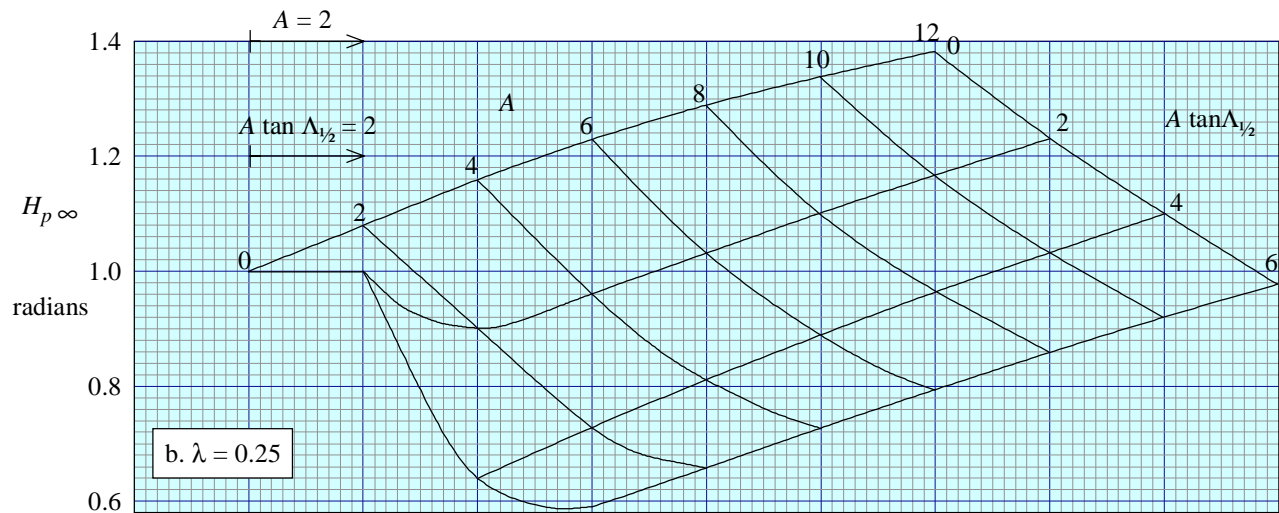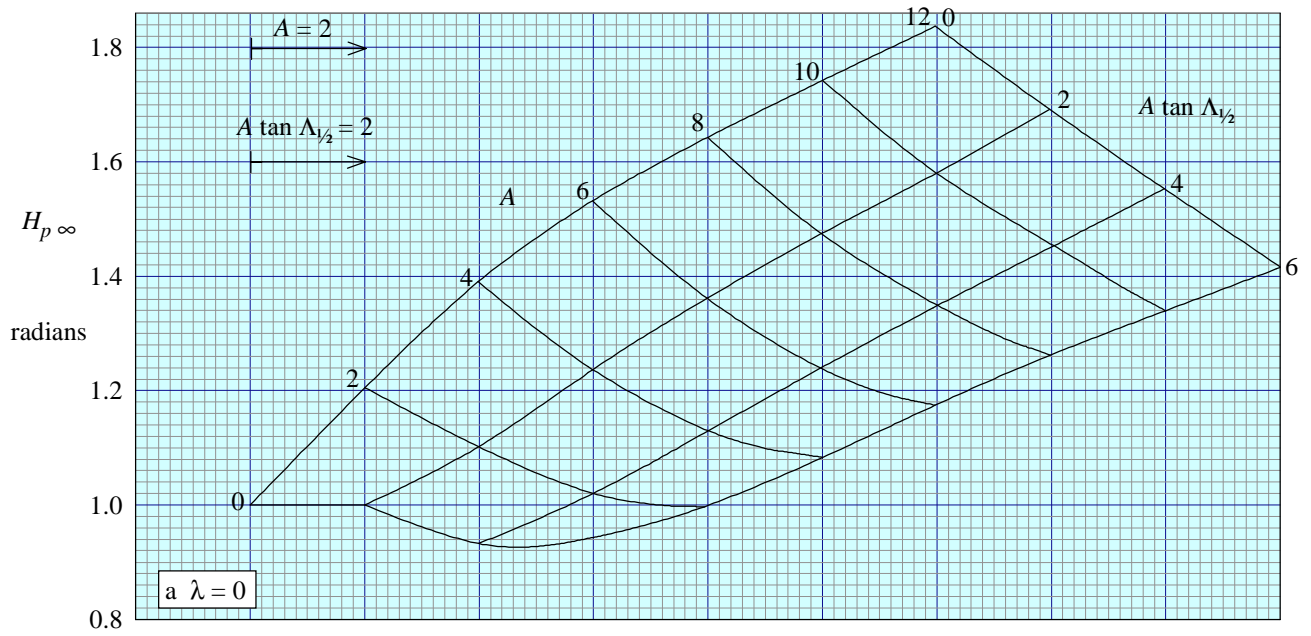
FIGURE 1 DOWNWASH PARAMETER AT AN INFINITE DISTANCE DOWNSTREAM

c. λ = 0.5

d. λ = 1.0
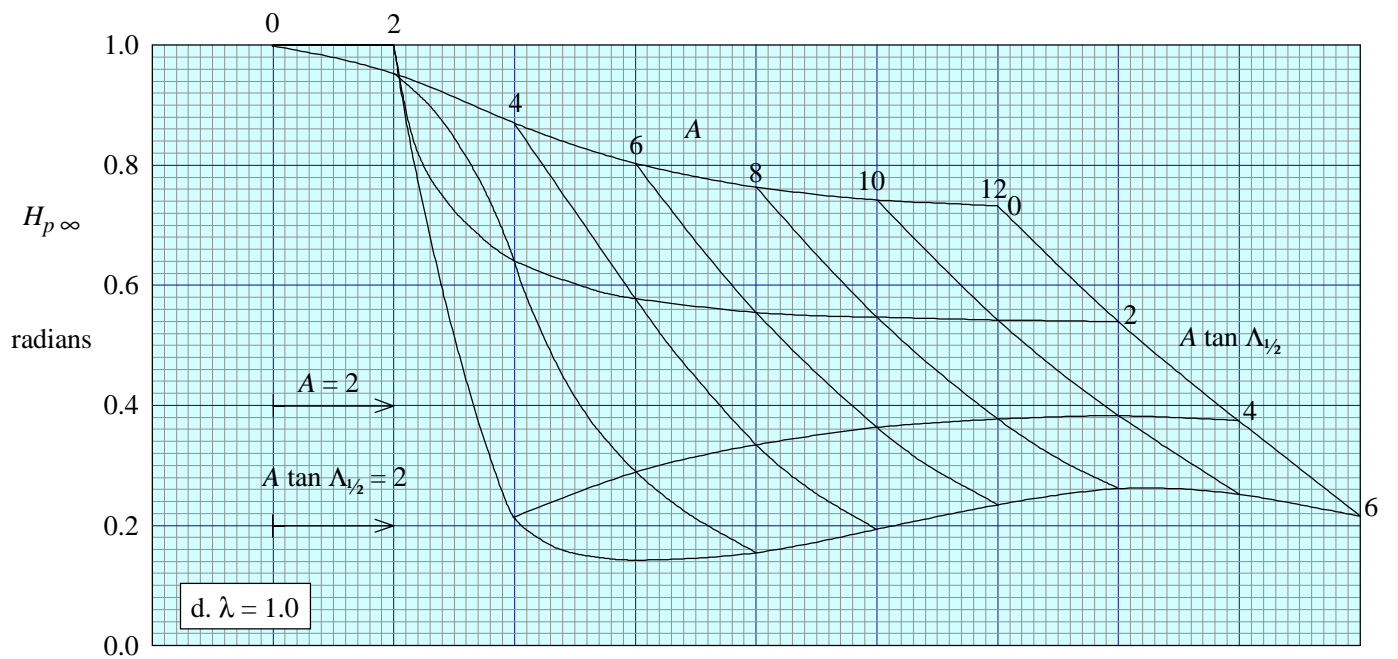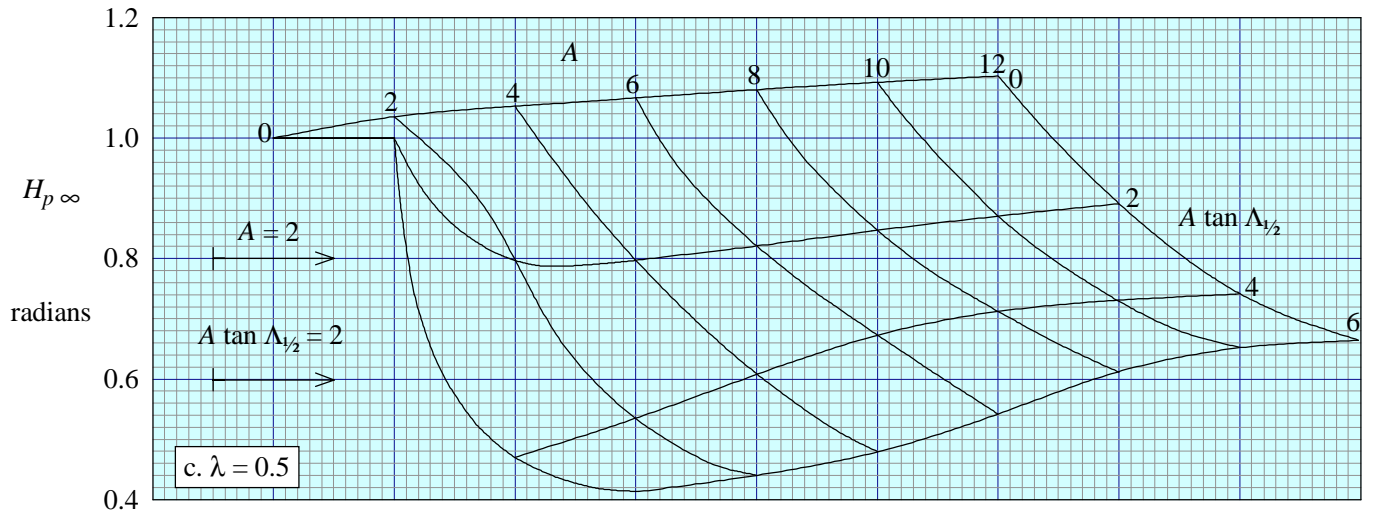
FIGURE 1 (concluded)
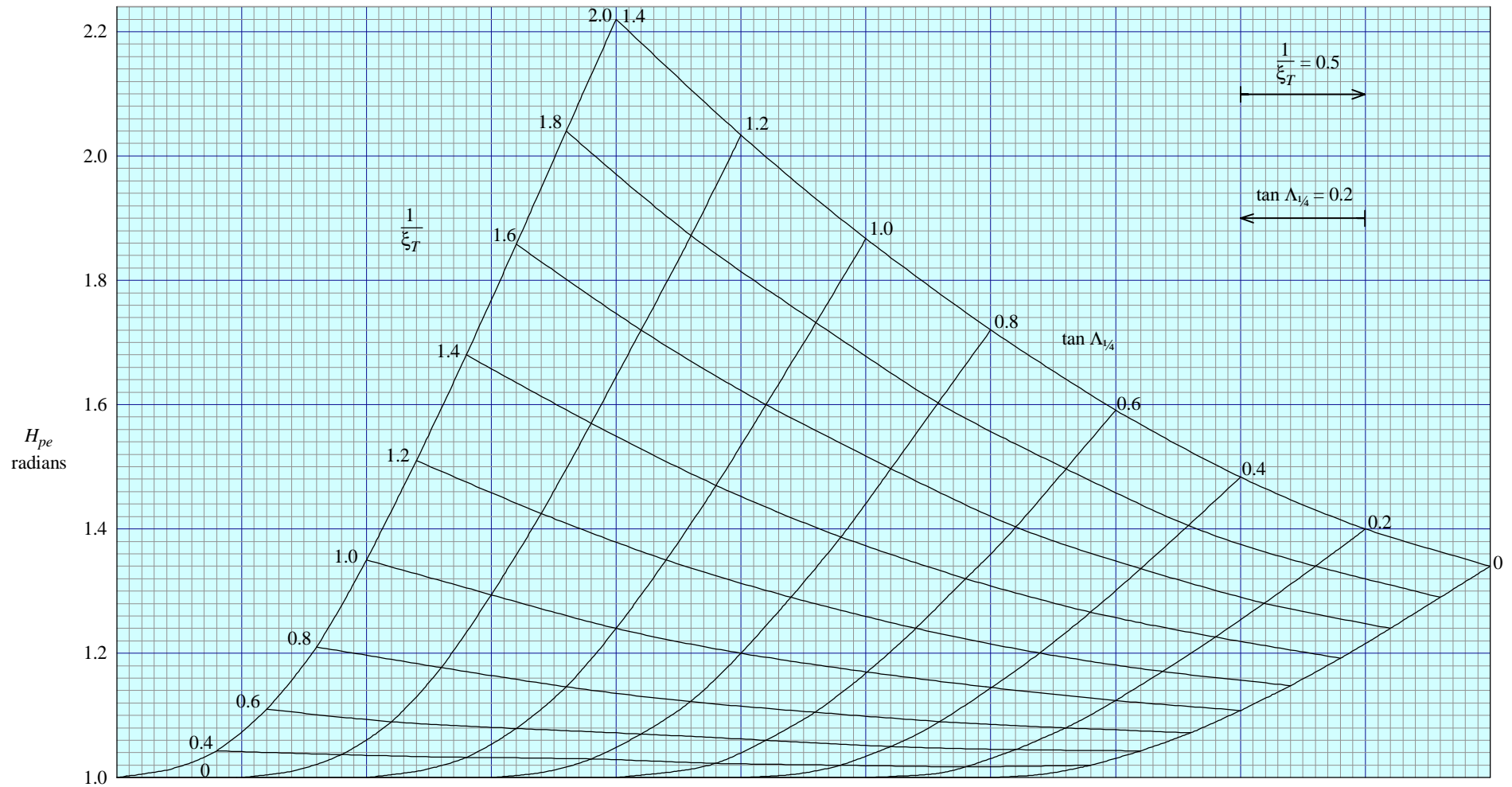
FIGURE 2 DOWNWASH PARAMETER FOR ELLIPTIC LOADING
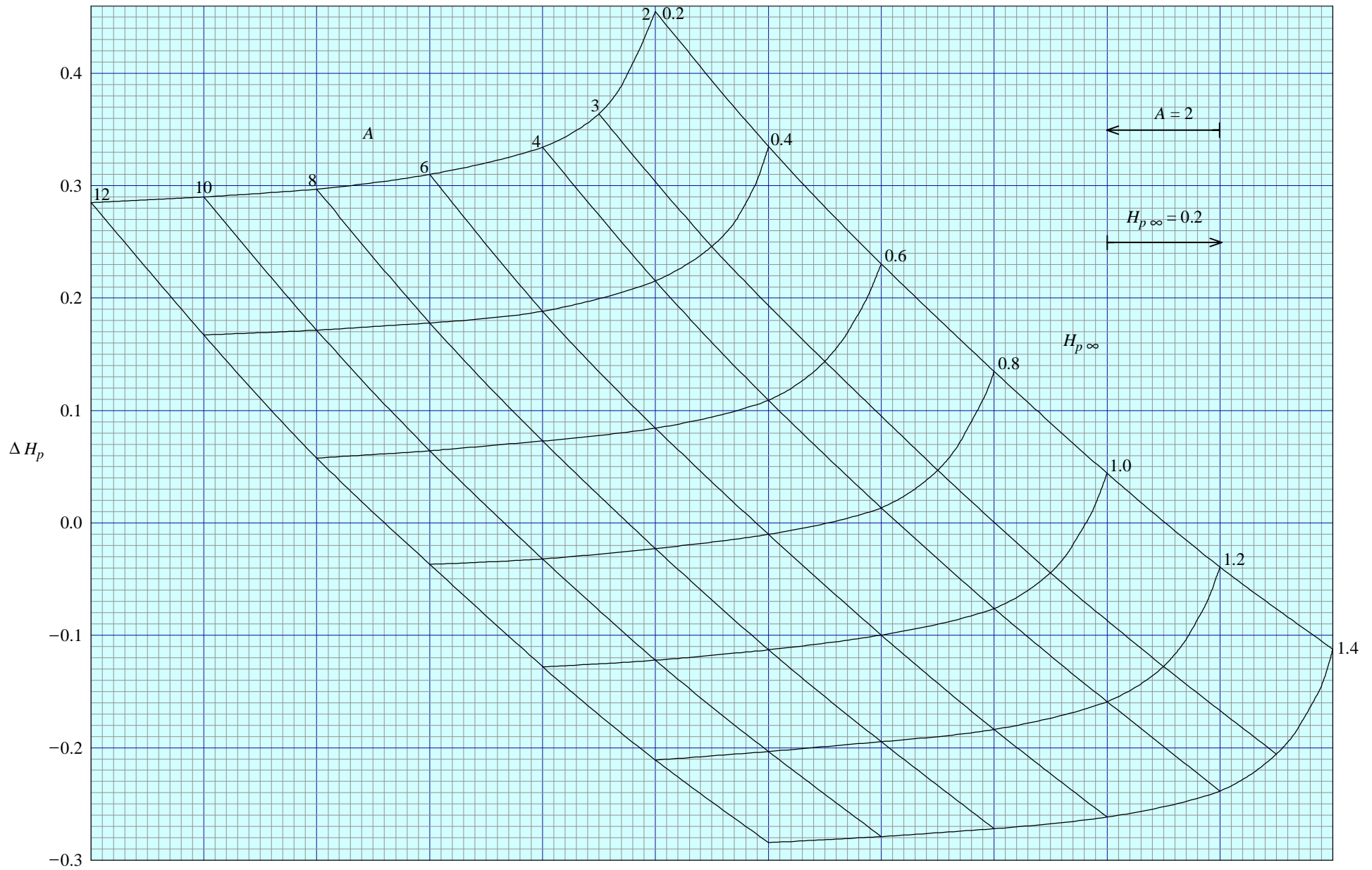
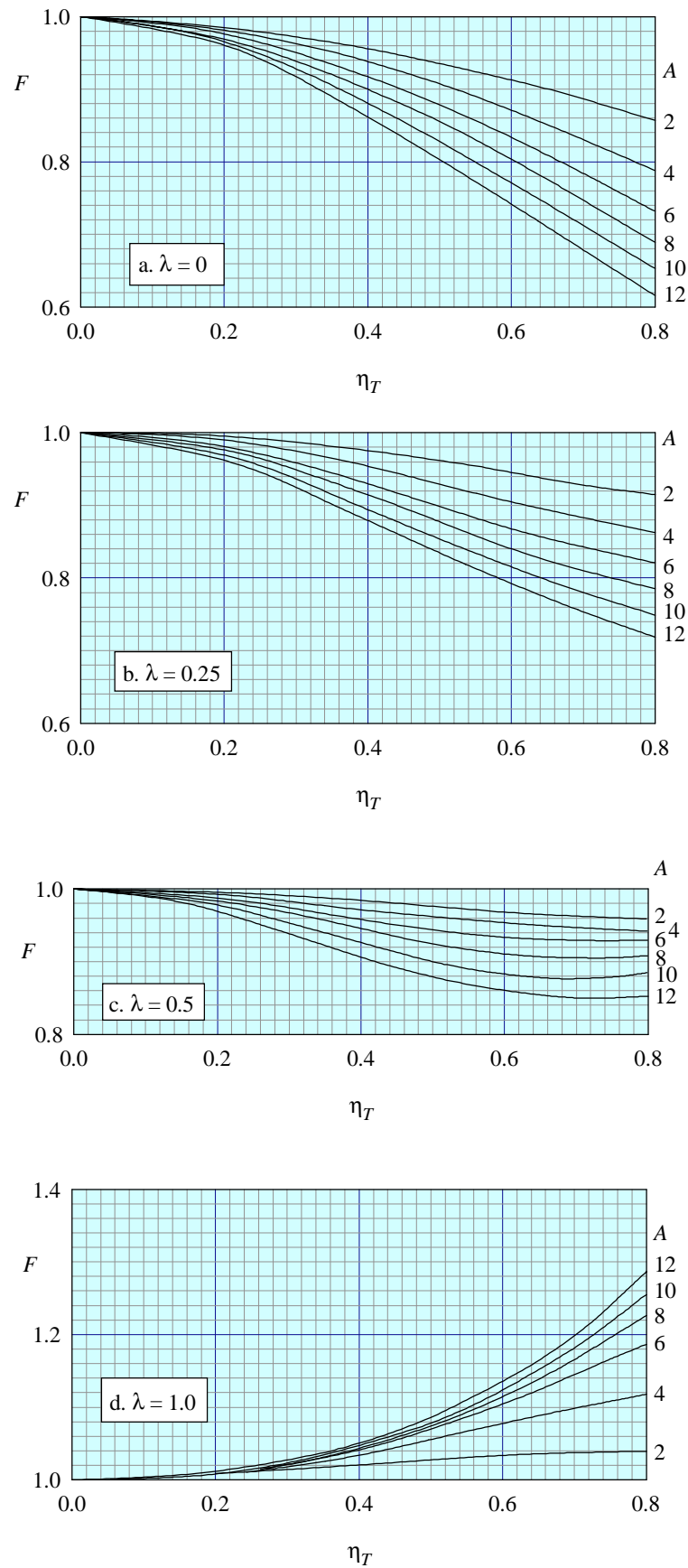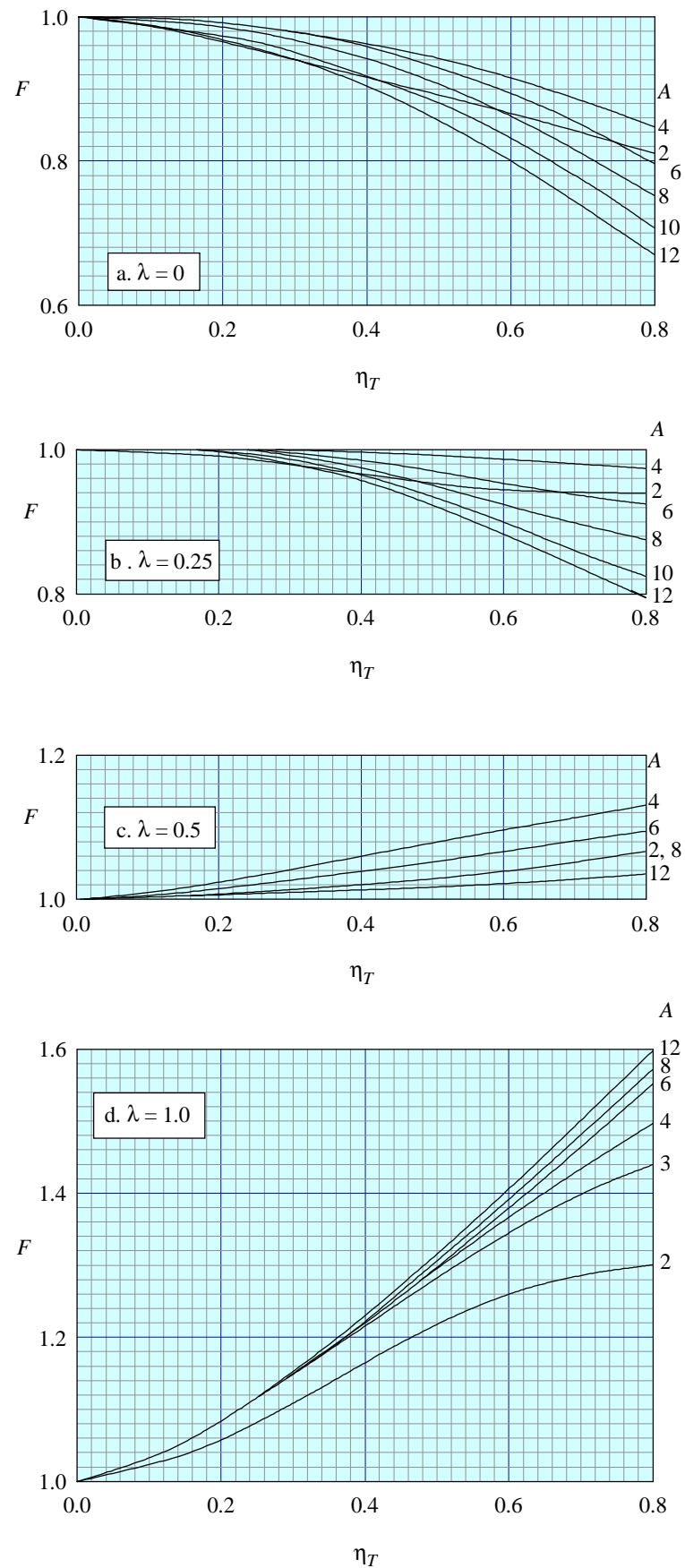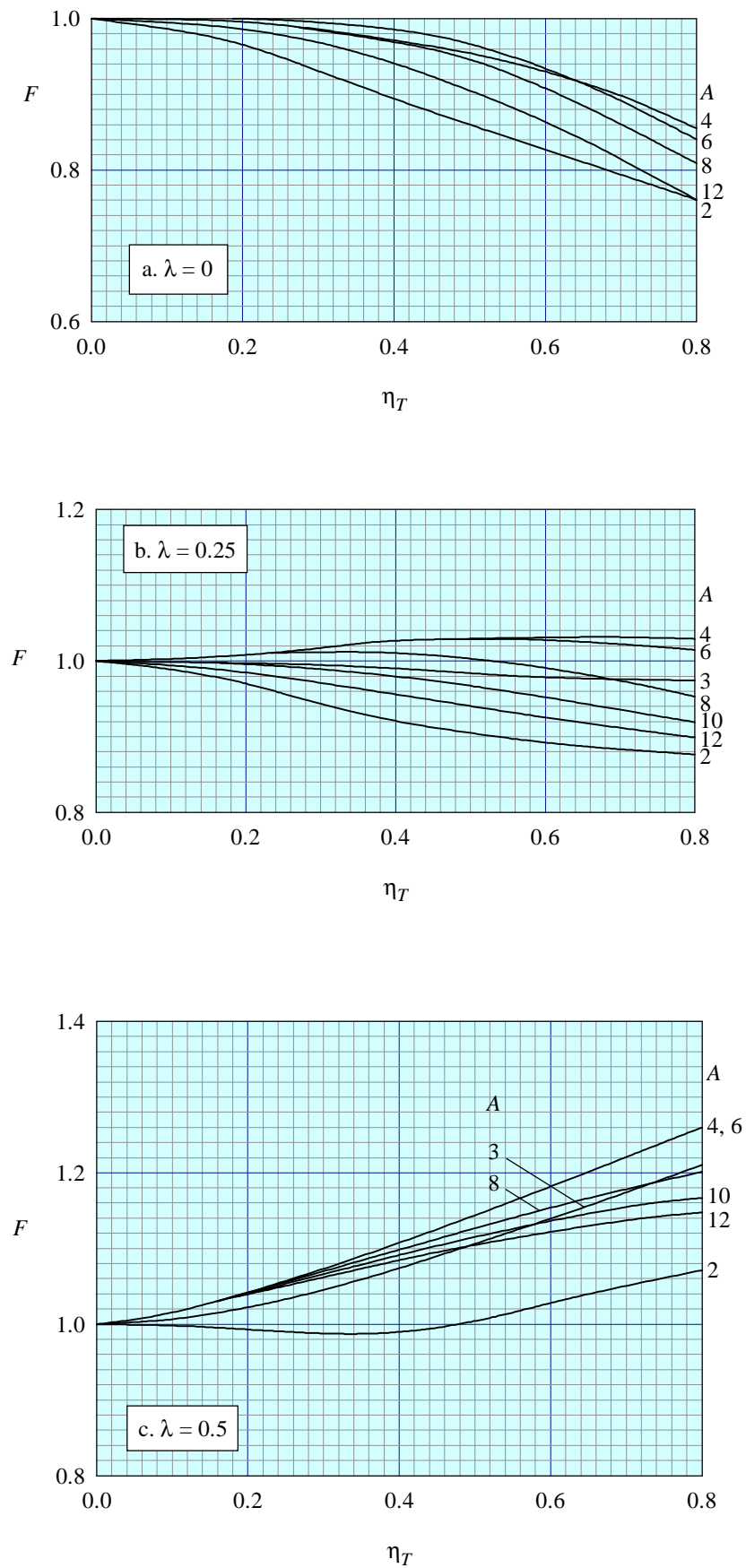**FIGURE 3 CORRECTION TO DOWNWASH PARAMETER**

FIGURE 4 FACTOR FOR AVERAGE DOWNWASH ACROSS TAILPLANE : $A \tan\Lambda_{1/2} = 0$

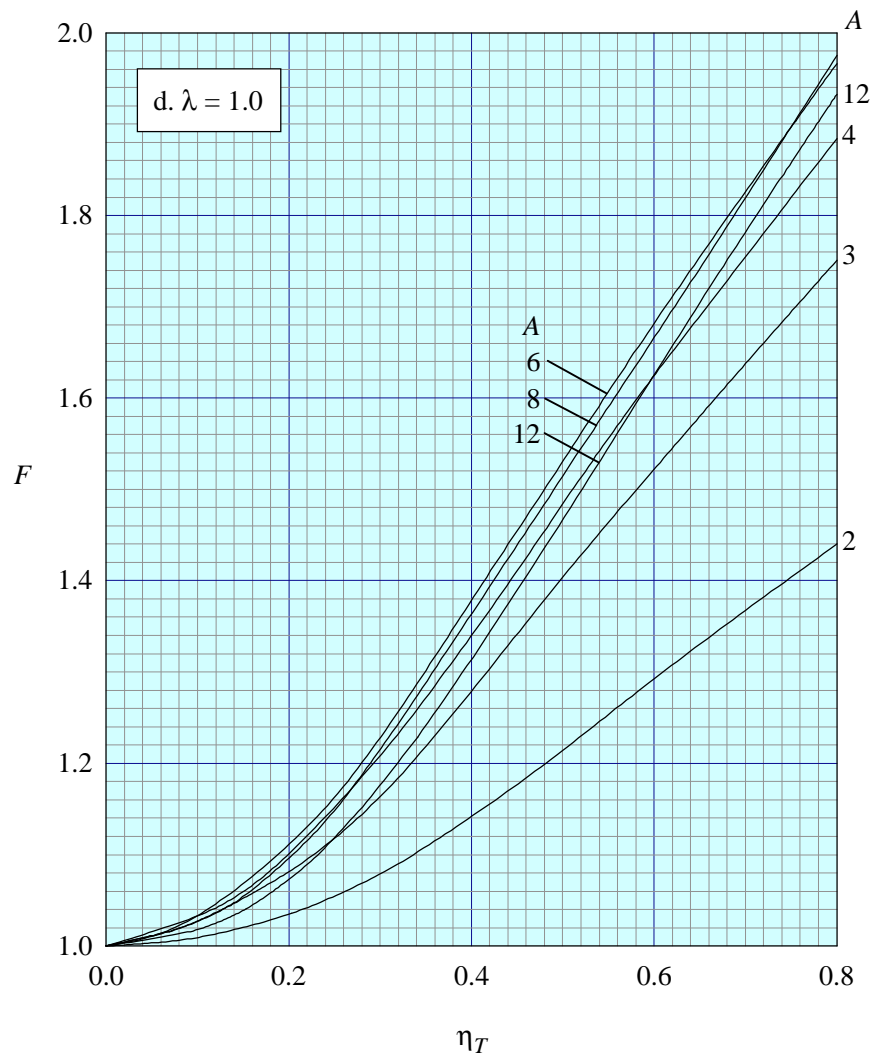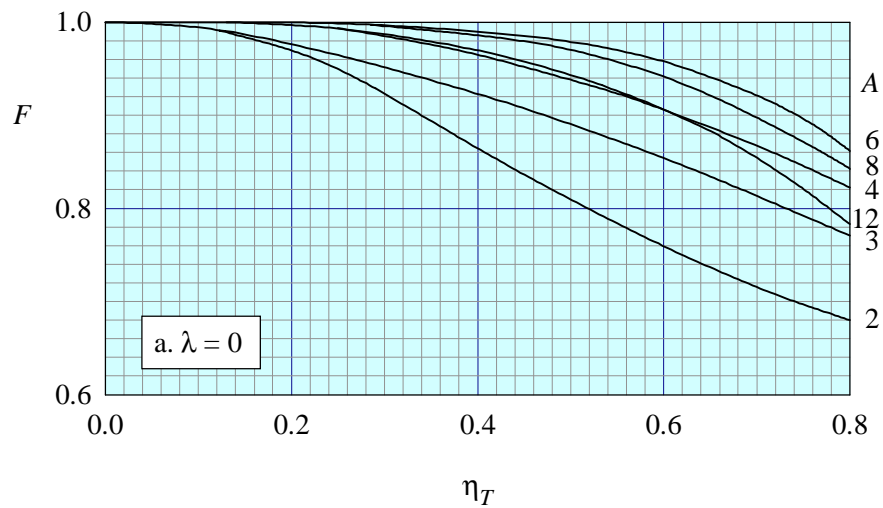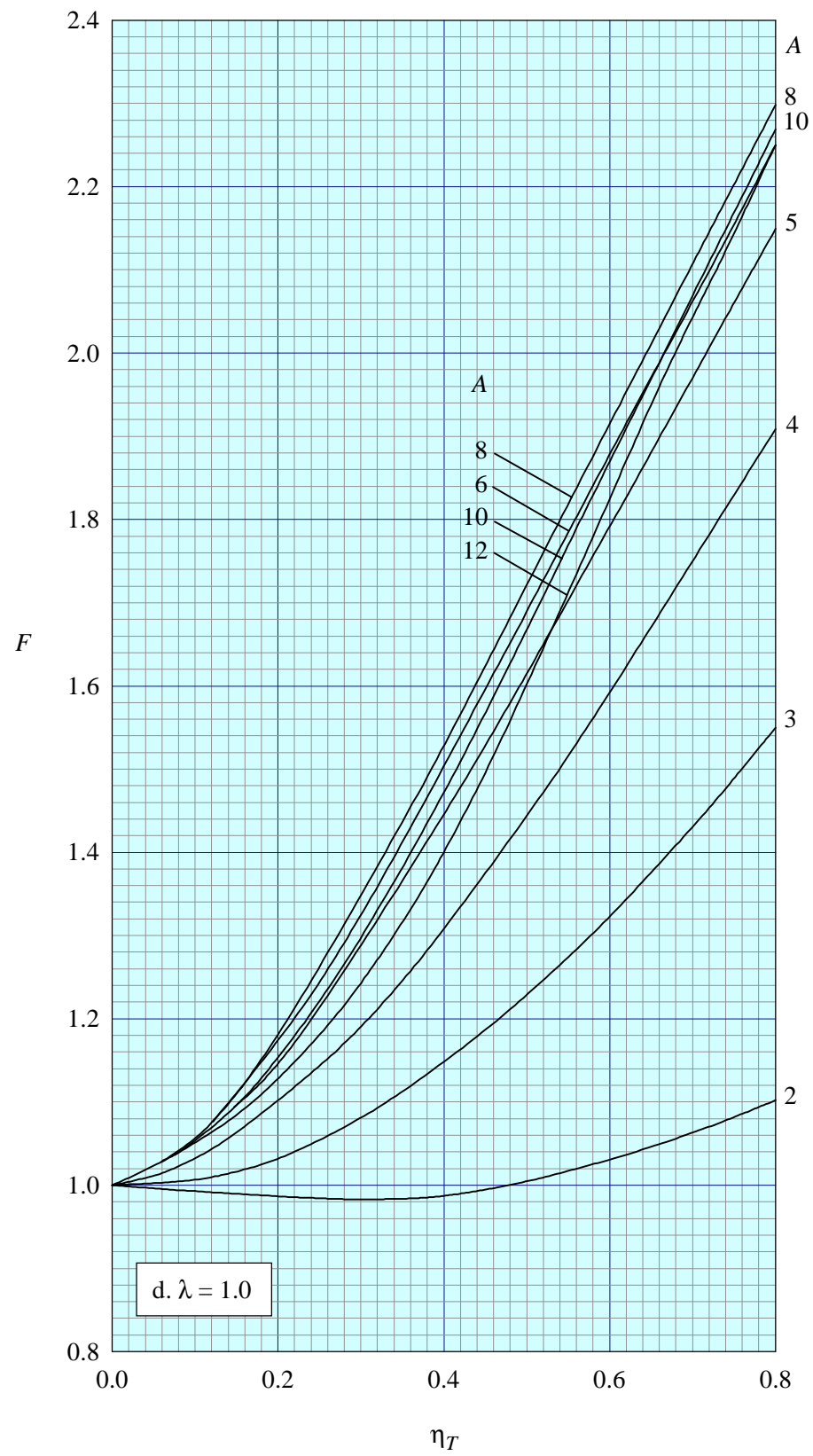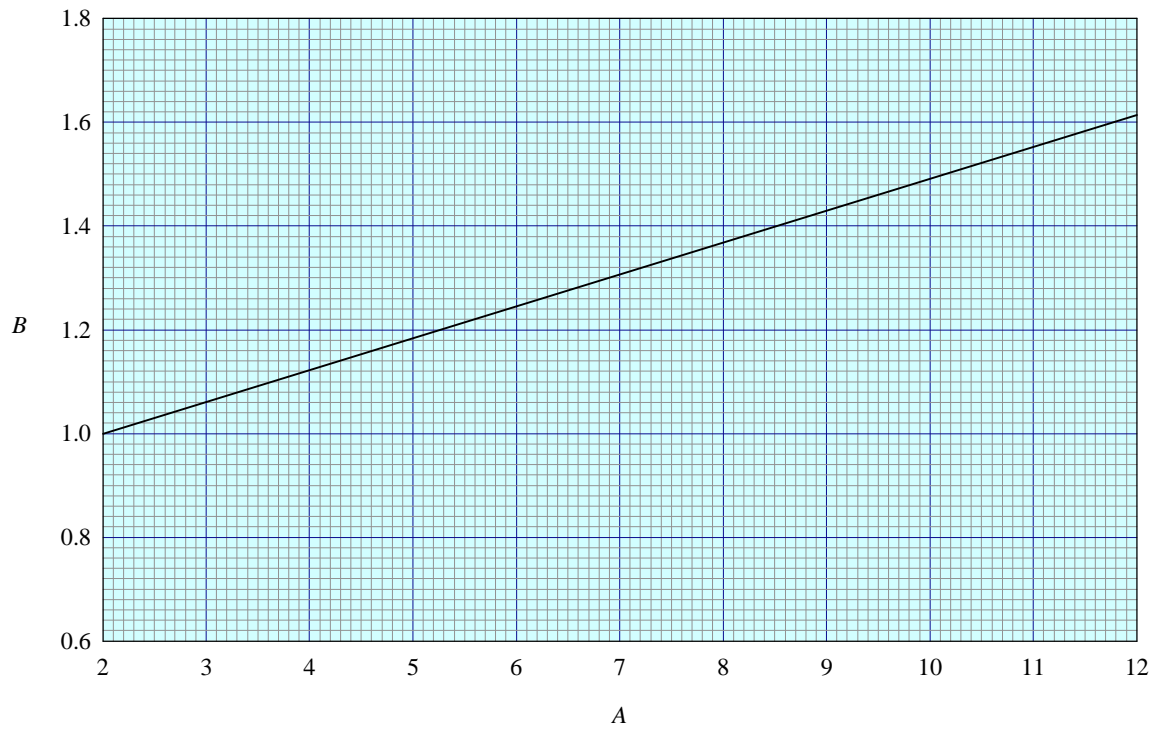**FIGURE 5 FACTOR FOR AVERAGE DOWNWASH ACROSS TAILPLANE :** $A \tan \Lambda_{\frac{1}{2}} = 2$

FIGURE 6 FACTOR FOR AVERAGE DOWNWASH ACROSS TAILPLANE : $A \tan\Lambda_{1/2} = 4$

FIGURE 6 (Concluded)

d. $\lambda = 1.0$

F

η_T

A

a. $\lambda = 0$

F

η_T

A

FIGURE 7 FACTOR FOR AVERAGE DOWNWASH ACROSS TAILPLANE : $A\tan\Lambda_{1/2} = 6$
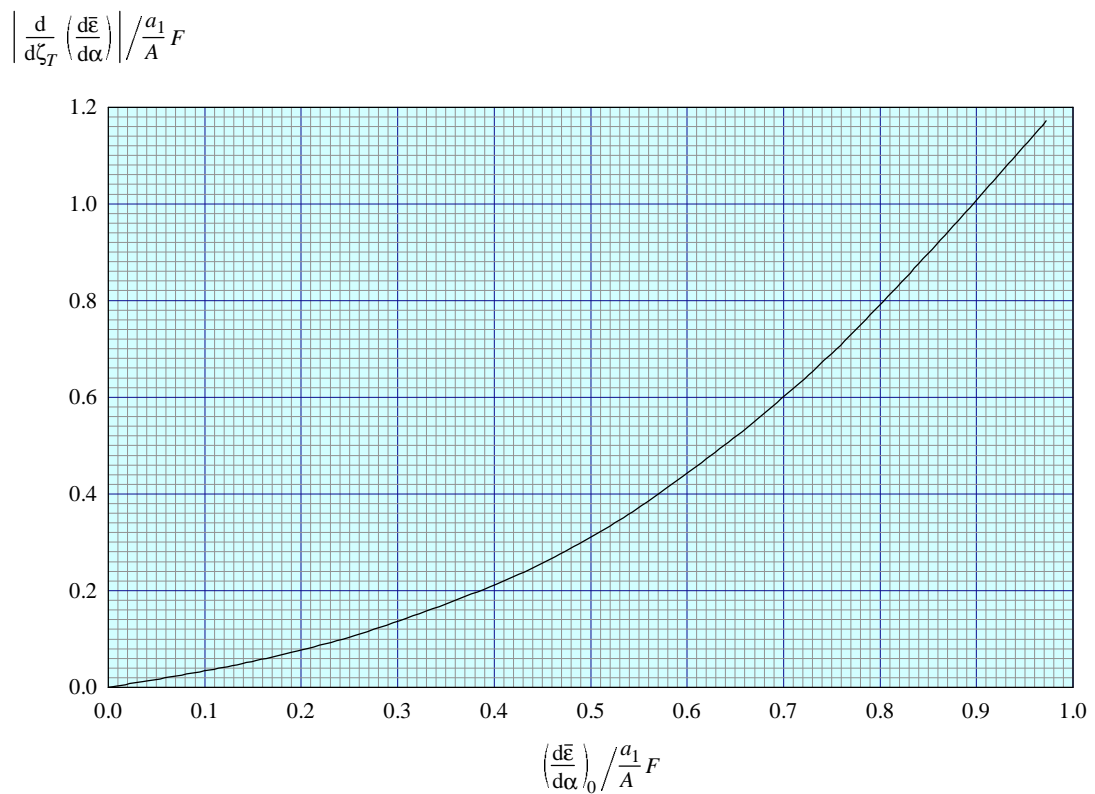
b. λ = 0.25

c. λ = 0.5
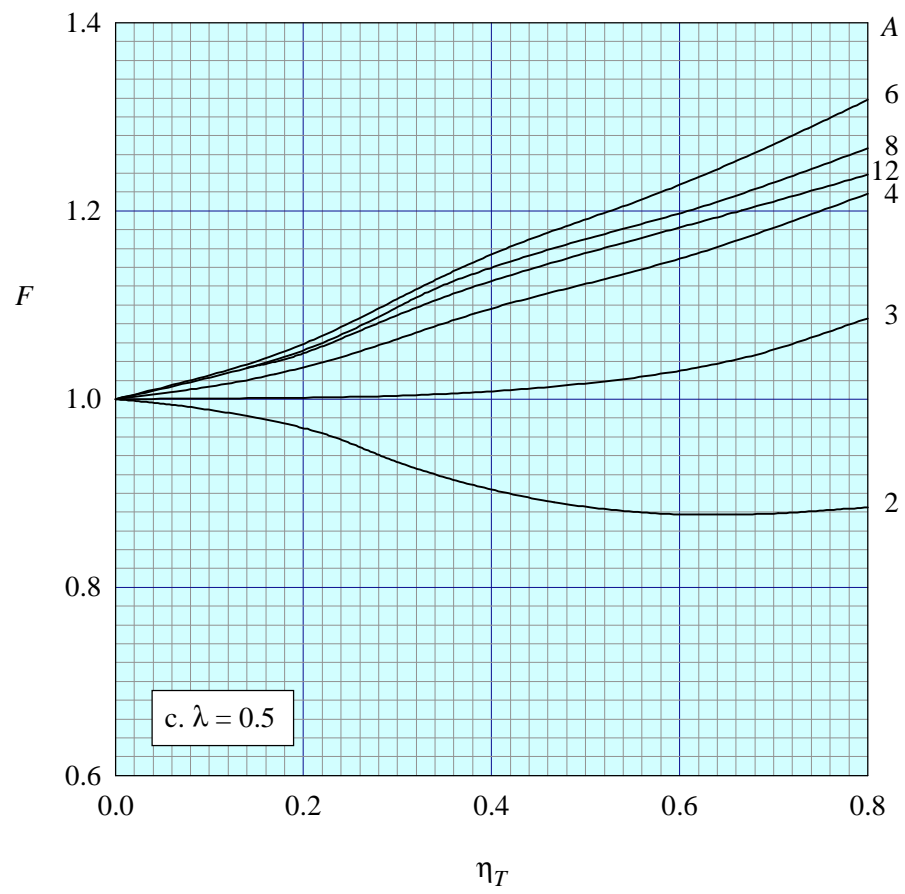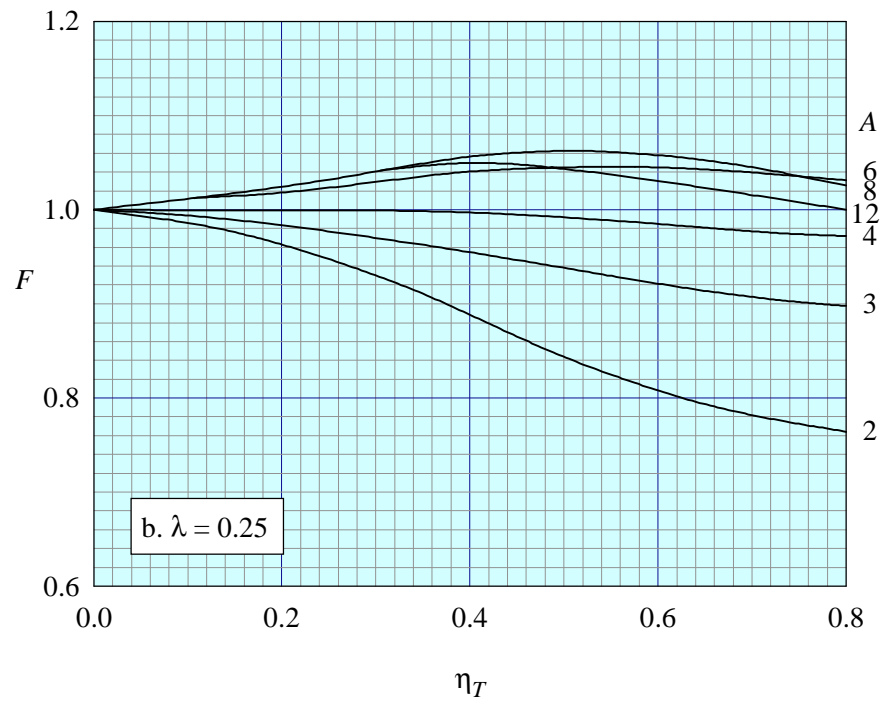
FIGURE 7 (continued)

FIGURE 7 (concluded)

FIGURE 8 EFFECT OF BODY ON $\left(\dfrac{d\bar{\varepsilon}}{d\alpha}\right)_0$

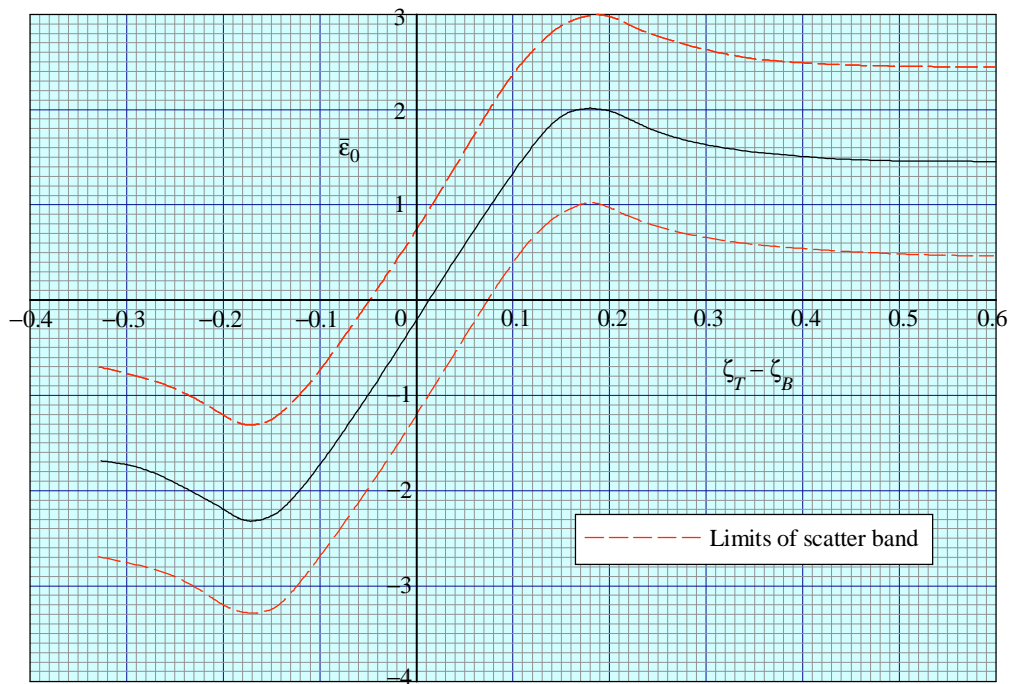FIGURE 9 EFFECT OF TAILPLANE HEIGHT ON $\dfrac{d\bar{\varepsilon}}{d\alpha}$
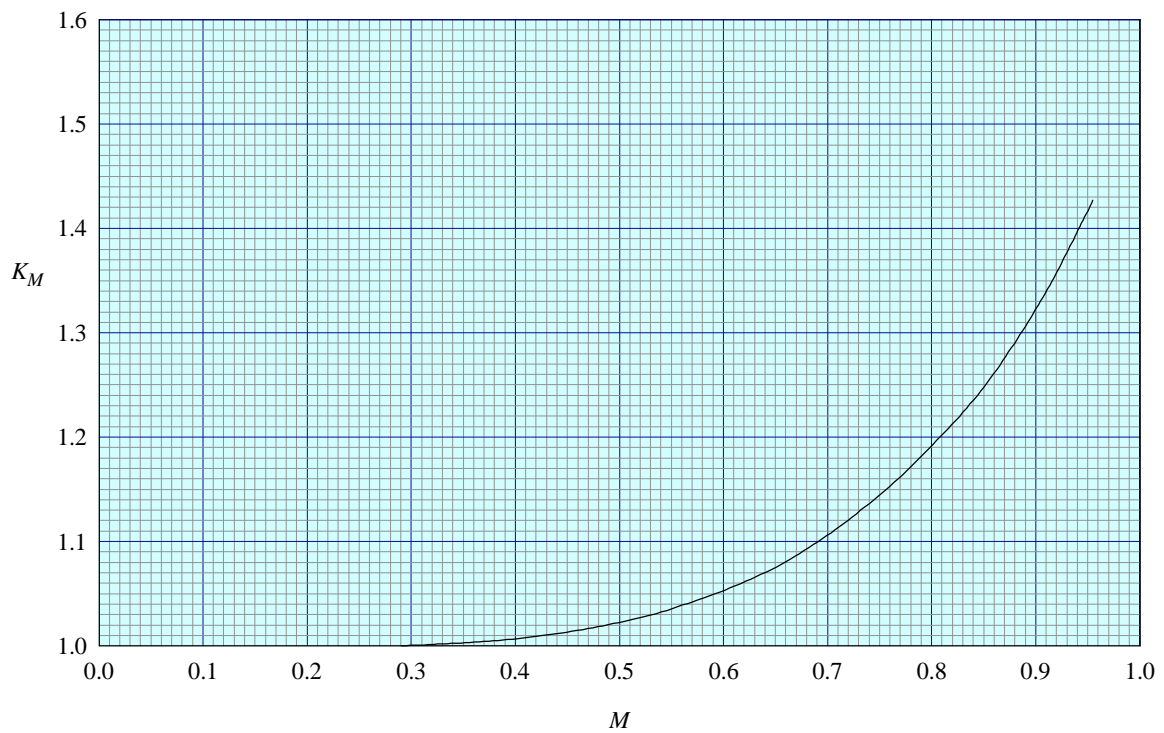
FIGURE 10 DOWNWASH AT ZERO LIFT

FIGURE 11 MACH NUMBER EFFECT ON $\dfrac{\mathrm{d}\bar{\varepsilon}}{\mathrm{d}\alpha}$

THE PREPARATION OF THIS DATA ITEM

The work on this particular Item, which supersedes Item Nos Aero A.08.01.02 to 04, was monitored and guided by the Aerodynamics Committee which first met in 1942 and now has the following membership:

Chairman
Mr P.K. Jones   – British Aerospace, Manchester Division

Vice-Chairman
Mr J. Weir   – Salford University

Members
Mr D. Bonenfant   – Aérospatiale, Toulouse, France
Mr E.A. Boyd   – Cranfield Institute of Technology
Mr K. Burgin   – Southampton University
Mr E.C. Carter   – Aircraft Research Association
Mr J.R.J. Dovey   – British Aerospace, Warton Division
Dr J.W. Flower   – Bristol University
Mr H.C. Garner   – Royal Aircraft Establishment
Mr A. Hipp   – British Aerospace, Stevenage-Bristol Division
Dr B.L. Hunt[*]   – Northrop Aircraft Group, Hawthorne, Calif., USA
Mr J. Kloos[*]   – Saab-Scania, Linköping, Sweden
Mr J.R.C. Pedersen   – Independent
Mr I.H. Rettie[*]   – Boeing Aerospace Company, Seattle, Wash., USA
Mr F.W. Stanhope   – Rolls-Royce Ltd, Derby
Mr H. Vogel   – British Aerospace, Weybridge-Bristol Division.

[*]   Corresponding Member

The member of staff who undertook the technical work involved in the initial assessment of the available information and the construction and subsequent development of the Item was

Mr P. D. Chappell   – Head of Aircraft Aerodynamics Group.